Global evaluation of large earthquake energy from 1997 through mid-2010

J. A. Convers[1] and A. V. Newman[1]

Received 12 August 2010; revised 21 April 2011; accepted 5 May 2011; published 6 August 2011.

[1] We develop an updated radiated seismic energy E catalog of global earthquakes with seismic moment $M_0 \geq 10^{19}$ Nm ($M_W \geq 6.7$) from 1997 through mid-2010, recording 342 events using 17849 seismograms. Station-specific corrections and event duration–dependent total P wave group calculations allow for improved E determinations for large- and long-duration earthquakes. We find the global mean energy-to-moment ratio $\bar{\theta} = \log_{10}(E/M_0) = -4.59 \pm 0.36$. Robust deviations are found for thrust ($\bar{\theta}_T = -4.74$), strike-slip ($\bar{\theta}_{SS} = -4.44$), and normal ($\bar{\theta}_N = -4.51$) faulting events. For two regions with recent energy deficient tsunami earthquakes (TsE), we examine all large thrust earthquakes with $M_0 \geq 5 \times 10^{17}$ Nm ($M_W \geq 5.7$), to identify a regional characterization in their relative radiated energy-to-moment ratio. While thrust events along Java, Indonesia, the site of two TsE events in 1994 and 2006, are comparable ($\bar{\theta}_{T-JV} = -4.91$) to the global thrust average, events along the Middle America Trench (MAT), the site of the 1992 Nicaragua TsE, are consistently deficient ($\bar{\theta}_{T-MAT} = -5.15$). Along the MAT, a trend of increased deficiency in radiated energy to the southeast occurs in the direction of more rapid plate convergence. Global thrust mechanisms become increasingly deficient in radiated seismic energy at shallow depths, with TsE events representing the shallowest and most energetically deficient end-member of the events in the study. Results suggest thrust events are highly variable but tend to increase in apparent stress from about 15 kPa near the surface to 2 MPa near 70 km depth.

Citation: Convers, J. A., and A. V. Newman (2011), Global evaluation of large earthquake energy from 1997 through mid-2010, *J. Geophys. Res.*, *116*, B08304, doi:10.1029/2010JB007928.

1. Introduction

[2] Understanding the physics of earthquakes requires relating the dynamics of faulting with seismologically observable parameters. One of these observables is the radiated seismic energy E, as an indication of the total wave energy generated by the rapid rupture of an earthquake [e.g., *Venkataraman and Kanamori*, 2004]. Thus, E is a valuable parameter, useful for understanding the dynamic rupture, particularly in the case of large and complex slow source earthquakes. The radiated energy, and hence energy magnitude M_e [*Choy and Boatwright*, 1995], is also useful for rapid real-time hazard assessment and damage mitigation as it does not saturate, and only requires the arrival of the initial P wave group for determinations in as little as 5 to 10 minutes at near-teleseismic distances (25° to 50°) (A. V. Newman and J. A. Convers, A rapid energy-duration discriminant for tsunami earthquakes, submitted to *Geophysical Research Letters*, 2011).

[3] While the seismic moment M_0, and hence moment magnitude M_W [*Hanks and Kanamori*, 1979], is highly valuable as an estimate of the total static work done in an earthquake, in isolation it does not describe the dynamic component of earthquake rupture. Full determinations of seismic moment frequently require the inclusion of the full body wave and/or substantial surface wave data for analysis [e.g., *Ekström et al.*, 2005], though real-time estimates may be made using integrated P wave seismograms at teleseismic distances. This real-time adaptation, however, requires an assumption of constant stress drop for accurate moment estimations [*Tsuboi et al.*, 1995, 1999]. These issues make seismic moment in isolation less useful for real-time hazard assessment [e.g., *Choy and Boatwright*, 2009; *Beresnev*, 2009]. Because events with the same M_0 can have considerable differences in their radiated energy, damage evaluations based solely on M_0 may inaccurately characterize the true damage caused by an earthquake. This is particularly the case for both high stress earthquakes that have disproportionately energetic shaking given their M_0 [*Choy and Kirby*, 2004], and tsunami earthquakes (TsE hereafter), which can be energetically deficient by more than a factor of ten relative to global averages of E/M_0, due to their slow rupture [*Newman and Okal*, 1998]. To better characterize the global distribution of earthquake energy release, we develop a catalog of recent earthquake energies and their energy-to-moment ratio using available broadband seismic recordings at teleseismic distances for events of $M_0 \geq 10^{19}$ Nm

[1]Department of Earth and Atmospheric Sciences, Georgia Institute of Technology, Atlanta, Georgia, USA.

0148-0227/11/2010JB007928

($M_W \geq 6.7$), and include earthquakes up to 20 times larger in moment release than in previous systematic studies. Thus, by comparing the energy-to-moment ratio results of this study with those by *Ide and Beroza* [2001], we can evaluate whether earthquakes remain largely scale invariant for the largest observed events.

[4] A detailed earthquake energy catalog provides a reliable base to explore ruptures in other large events, with the possibility of real-time applications in tsunami warning and disaster mitigation. For real-time calculations, existing records of global and regional activity are useful for determining zones with anomalous behavior. The methodology applied here is useful for real-time detection of earthquakes through (1) a global improvement in the determination of average source and path characteristics; (2) identification and correction of station-specific deviations due to either local seismologic structure or potentially incorrect instrument responses; (3) identification of regional and tectonic controlled variations in source parameters; and (4) use of the real-time determined rupture duration.

2. Methodology

[5] This study is built upon the methods described by *Boatwright and Choy* [1986] and *Newman and Okal* [1998], but utilizes advancements in computational code for more rapid and automated processing, and it is benefited by the vast improvement in the readily available broadband seismic data from globally distributed stations.

2.1. Energy Calculation

[6] *Boatwright and Choy* [1986] developed a method to calculate the energy radiated from seismic waves using the shaking recorded in the *P* wave group ($P + pP + sP$). The group energy is selected because energy flux from individual phases overlap for shallow rupturing and long-duration earthquakes. For shallow earthquakes, the phases travel along similar paths and hence a group attenuation correction can be made. However, the *pP* and *sP* phases of deeper earthquakes become distinctly separated from the direct arrival, and are preferentially attenuated because the direct *P* phase no longer travels through the weak sourceside crust.

[7] From the velocity records, the energy flux can be computed in the time domain at each station, and integrated over the duration of the generalized *P* wave group. However, by calculating the per station energy flux in the frequency domain, it is possible to directly correct for frequency-dependent anelastic attenuation, obtaining a new theoretical station energy flux corrected for attenuation ε^* [*Boatwright and Choy*, 1986; *Newman and Okal*, 1998]:

$$\varepsilon^* = \frac{\rho\alpha}{\pi}\int_0^\infty |\omega u(\omega)|^2 e^{\omega t^*(\omega)} d\omega, \tag{1}$$

where ρ = 3000 kg/m^3 and α = 7 km/s are the approximate near-source density and compressional wave velocity for shallow earthquakes, respectively. The square of the velocity seismogram u and frequency-dependent attenuation correction t^* are integrated over the angular frequency ω. Represented in seconds, t^* is the reciprocal of the characteristic ω representing the frequency by which an exponential decay of energy is $1/e$ its original value [*Der et al.*, 1982]. The values of t^* used in this study were introduced by *Choy and Boatwright* [1995] and put in equation form by *Newman and Okal* [1998].

[8] We convert ε^* measured at each station back to radiated source energy E by correcting for each geometric spreading, the depth and mechanism-dependent coefficients for radiated energy in the *P* wave group, and the partitioning between *P* and *S* waves, similar to *Boatwright and Choy* [1986]. Our determination of the radiated earthquake energy at the source is then

$$E = (1+q)4\pi\left(R^P\right)^2 \frac{\left\langle \left(F^P\right)^2 \right\rangle}{\left(F^{gP}\right)^2} \varepsilon^*, \tag{2}$$

where q = 15.6 is the relative partitioning between *S* and *P* waves [*Boatwright and Fletcher*, 1984], R^P is the distance-dependent geometric spreading coefficient, $\langle (F^P)^2 \rangle$ = 4/15 is the average squared radiation pattern of the direct *P* wave [*Aki and Richards*, 1980], and F^{gP} is the mechanism-dependent radiation coefficient of the *P* wave group including *pP* and *sP* given by *Boatwright and Choy* [1986]. Though F^{gP} is near 1 for dip-slip mechanisms, we require $F^{gP} \geq 0.2$ to avoid a near singularity that exists at distal stations ($\Delta > 60°$) for strike-slip mechanisms where the takeoff orientation becomes near nodal for the direct *P* and depth phase arrivals.

[9] While the energy should ideally be calculated across an infinite frequency range (according to equation (1)), digital recordings, anelastic attenuation, and the finiteness of the processing window limit the feasible range of calculation. To maintain consistency with the previous catalog of *Newman and Okal* [1998], we limit the frequency range to between 14 mHz and 2 Hz (period range between 0.5 and 70 s). At frequencies above 2 Hz much of the signal falls below background noise levels, particularly for smaller events [e.g., *Choy and Boatwright*, 1995; *Newman and Okal*, 1998; *Vassilou and Kanamori*, 1982]. The lower frequency limit of 14 mHz is chosen because it corresponds to the time window of evaluation (70 s) of *Newman and Okal* [1998], and is maintained for catalog comparisons.

[10] For many of the larger ($M_W > 7.8$), and deep (depth > 70 km) earthquakes, directivity is observable with increased strong shaking and shorter duration in the direction of rupture. Fortunately, directivity does not seem to significantly impact the teleseismic estimates of radiated energy [*Venkataraman and Kanamori*, 2004]. By taking advantage of available waveforms from stations within numerous permanent networks we improve estimates of E by further minimizing azimuthal dependency that may arise from directivity, inaccuracies in focal mechanisms, regional variations in attenuation, and individual station response issues.

[11] In practice, teleseismic vertical recordings (epicentral distance between 30° and 80°) are used from broadband seismic stations. For a few events, stations as close as 25° were used without visibly increased errors (Figure 1), however it should be noted that recordings from stations nearer than 30° are potentially complicated by triplication of arrivals due to the shallow takeoff angle, and contamination from reflected *PP* energy. Additionally, recordings from stations at distances greater than 80° may have reduced signal for smaller events and can reflect rapidly lost energy because of diffraction around the outer core, and are thus avoided. The

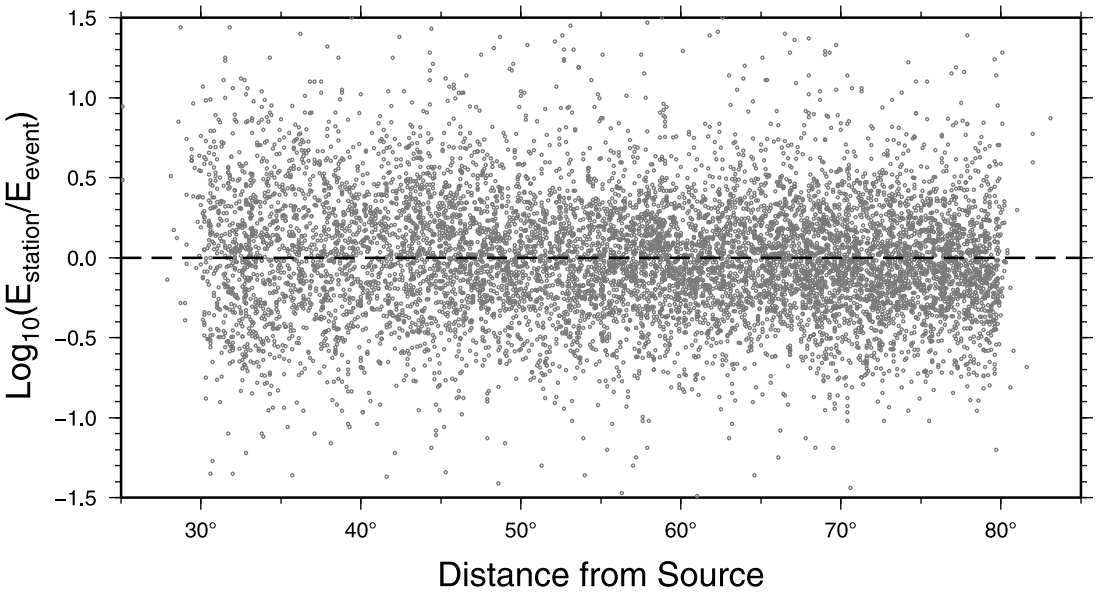

Figure 1. To evaluate the potential for distance dependence in E solutions, we show the per station E deviation as a function of distance for all events shallower than 30 km (deeper earthquakes are excluded because of the relatively shallow takeoff in the near field). No significant trend is observed, suggesting that determinations are largely robust and not particularly sensitive to energy contamination from other arrivals including *PP* (<30°), and *PcP* (>50°), when calculating energy to 70 s.

largely consistent E deviations observed across all distances used in this study suggests that contamination from later arrivals (including *PP*, *PcP*, etc.) are not substantial (Figure 1).

[12] The stations used are those available from 51 networks (networks used are AD, AK, AT, AU, AV, AZ, BK, CC, CI, CN, CU, CZ, G, GB, GE, GR, GT, HL, HW, IC, II, IU, IW, JP, KN, KZ, LB, LD, LI, LX, MN, MS, MY, NE, NL, NM, NN, NO, PE, PM, PN, PR, PS, SS, TA,TS, TW, UO, US, UW, and XG) readily available from the Incorporated Research Institutions for Seismology (IRIS) Data Management Center (DMC). Because of vast improvements in global station coverage, final energy determinations are made with 52 stations on average. This represents a significant improvement over *Newman and Okal* [1998] and *Weinstein and Okal* [2005], which use 10 and 27, respectively, and a modest improvement over the ongoing U.S. Geological Survey determinations [*Choy and Boatwright*,

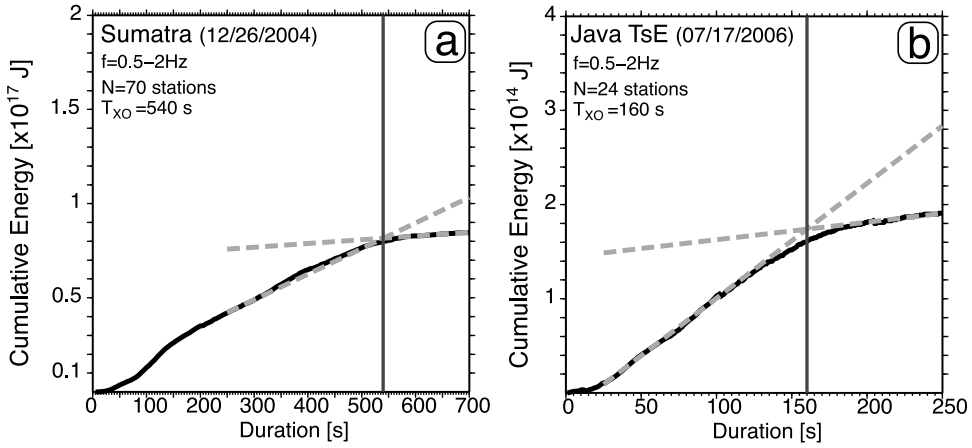

Figure 2. Cumulative high-frequency energy growth (0.5–2 Hz), as a function of time for (a) the M_W 9.1 Sumatra 2004 earthquake and (b) the M_W 7.8 Java 2006 tsunami earthquake (TsE). The per second averaged energy growth across all stations shows an initial ramp-up in the first 100 s and 20 s for the Sumatra and Java events, respectively, before increasing at a near-constant and independent energy rate before falling off to a much reduced background growth. The crossover time T_{XO}, approximating the rupture duration, is the crossover between linear growth and die-off slopes. Note that utilizing only the initial 70 s energy would underestimate the energy determination of the Sumatran earthquake by more than a factor of 6, and the Java TsE by more than a factor of 2.

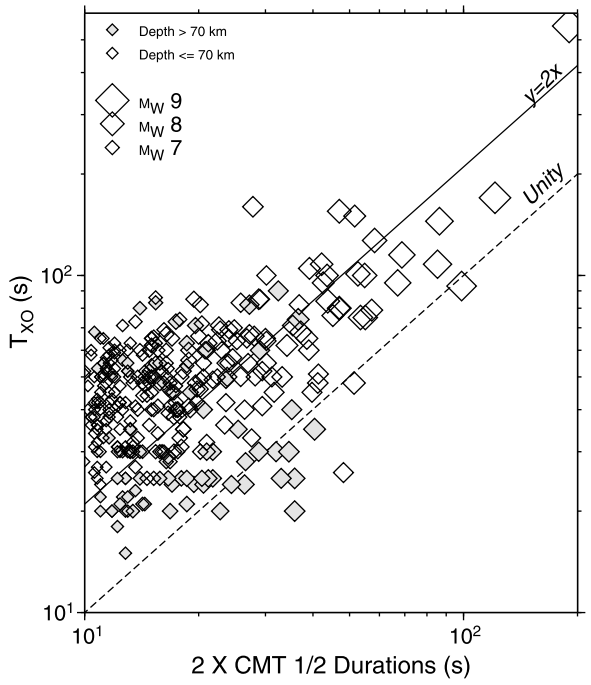

Figure 3. Duration estimates for shallow (open symbols) and deep (filled symbols) earthquakes in the global catalog are shown relative to twice the half-duration estimates from the gCMT catalog. The latter are fixed in gCMT inversions, hence they are not necessarily representative of the full duration [*Ekström et al.*, 2005]. On average, durations determined here are twice of those within the gCMT, but have considerable scatter.

1995], which used ~45 stations on average in energy determinations over the same time period.

2.2. Duration Determination

[13] Because some large earthquakes have rupture durations that far exceed the 70 s window of evaluation in the *Newman and Okal* [1998] study, most notably the approximately 540 s rupture of the 2004 Sumatran earthquake [*Ammon et al.*, 2005; *Weinstein and Okal*, 2005; *Ni et al.*, 2005], it was necessary to adapt the method to all events for variable source durations. This is achieved by making averaged incremental measurements of energy starting with the initial *P* arrival while also increasing the window of the waveforms analyzed by 1 s increments. The incremental measurements are continued for at least 100 s beyond the expected event duration (normally ran to 300 s), and the per second cumulative energy growth of each station is averaged to examine the composite energy growth of an event (Figure 2). The rupture duration is approximated by identifying the point of maximal falloff in the growth of high-frequency rupture energy (between 0.5 and 2 Hz) as described by A. V. Newman and J. A. Convers (submitted manuscript, 2011) and similar to *Lomax et al.* [2007]. The 0.5 to 2 Hz band is chosen because it avoids much of the energy from later arrivals that are largely attenuated in this frequency band [*Ni et al.*, 2005].

[14] The aptly named crossover duration T_{XO} is estimated as the crossover from the near-constant increasing energy rate to the relative flat and slow continued growth due to scattered energy including later arrivals (A. V. Newman and J. A. Convers, submitted manuscript, 2011). Examples of the duration determination for the M_W 9.1 Sumatra 2004 earthquake and the M_W 7.8 Java TsE are shown in Figure 2. T_{XO} is shown here as the intersection of two linear fits to the rapid increase and the near-horizontal die-off of energy growth. While the method is particularly helpful for long-duration events, it modestly overestimates the duration of smaller events, and deeper earthquakes (A. V. Newman and J. A. Convers, submitted manuscript, 2011). In the case of deep events (depth $\geq$ 70 km), care must be taken to not miss the later arrivals of *pP* and *sP* energy which would appear as a second corner in the energy growth, becoming more separated the deeper the event occurs. Estimated T_{XO} values are reported for all events in Table S1 of the auxiliary material, and are shown relative to the global Centroid Moment Tensor (gCMT) estimated durations (2x the reported half duration) in Figure 3 [*Ekström et al.*, 2005].[1]

[15] While results for larger earthquakes are largely consistent, the T_{XO} has a tendency to overestimate durations relative to the gCMT solutions, which are largely empirical for many of these events and based solely on M_W. There are two main causes for this: (1) for smaller events, the latency of energy from the depth phases (pP and sP) becomes large relative to the rupture duration (e.g. adding approximately 15 s to events at 30 km depth); and (2) site-specific scattered energy can contribute to significant late energy at some individual stations causing a bias that again becomes apparent for shorter-duration ruptures. To reduce these errors one could consider applying a depth-dependent correction, or down-weighting the contribution from stations that report artificially long durations in an event's final duration determination.

[16] The resultant determination of T_{XO} from the high-frequency cumulative energy growth is used as the cutoff time for our estimation of total radiated energy for all earthquakes. While for small earthquakes, this value has little effect on the final energy estimation (note the near flat continued growth after T_{XO} in Figure 2), it can greatly affect the results for very large earthquakes. In the case of the Sumatra 2004 event, the high-frequency energy was less than one-sixth the ultimate size when measured at the 70 s cutoff used by *Newman and Okal* [1998], rather than at T_{XO} = 540 s (Figure 2a).

[17] In the case of events with rupture durations longer than 70 s, the corner frequency will be below the minimum frequency of observation in this study (14 mHz). However, we find that the additional energy in these lower frequencies are mostly negligible. In the example of the 2006 Java TsE, which ruptured for approximately 160 s (Figure 2), the additional energy found in frequencies down to the earthquake's corner frequency (1/160 s = 6.25 mHz) was approximately 1% over that which was measured down to the minimum reported in this study. While in the most extreme case of the Giant 2004 Sumatran earthquake, which ruptured for approximately 540 s (Figure 2), energy calculations to the earthquakes approximate corner frequency (1/540 s = 1.85 mHz) yields 10% more energy. In each case, the addi-

[1] Auxiliary materials are available in the HTML. doi:10.1029/2010JB007928.

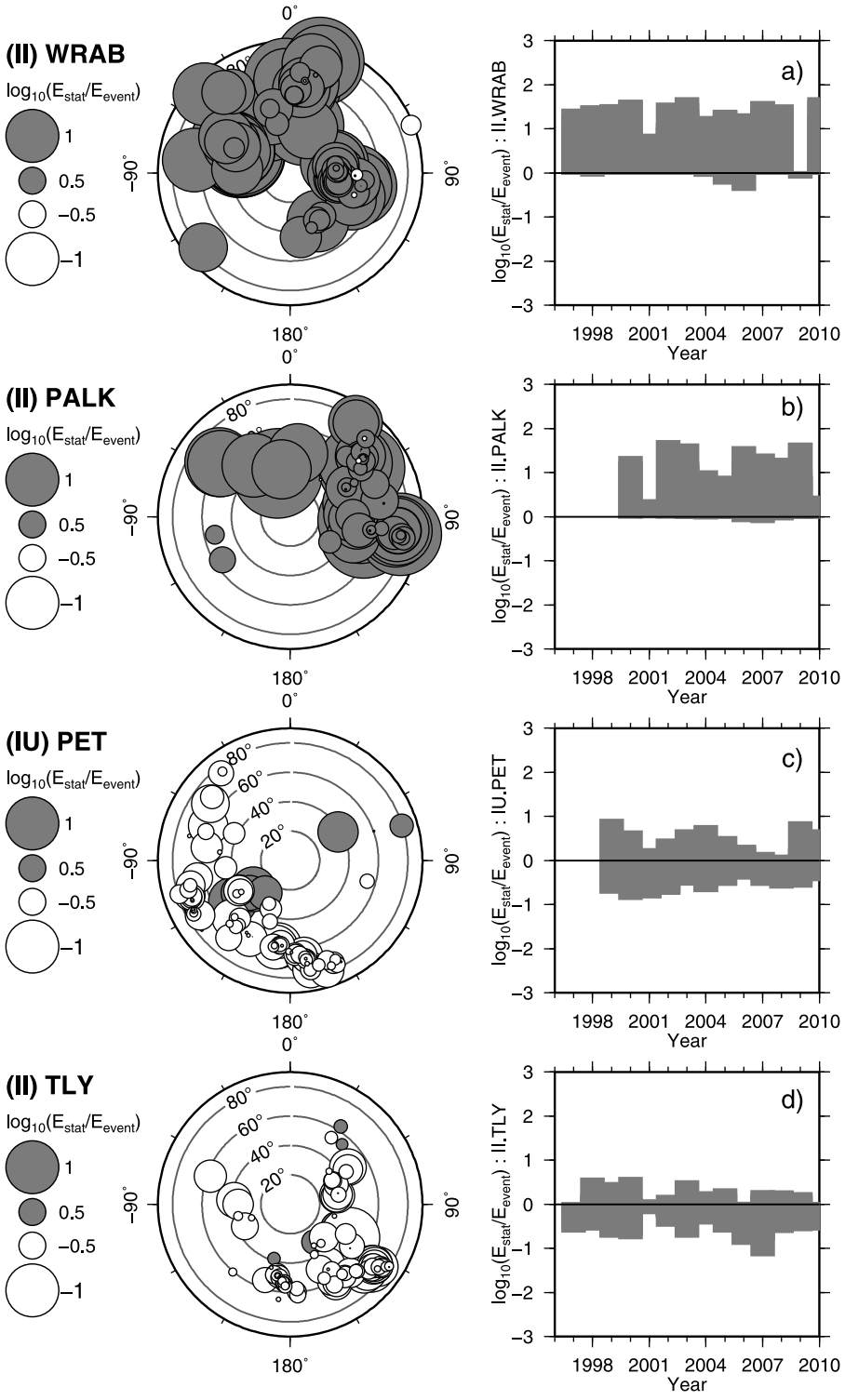

Figure 4. Four representative stations (rows), of the 1342 used for energy determinations, are shown with their (left) azimuthal and distance distribution of per event energy deviations, as well as (right) their temporal deviation. Two stations with little bias and relatively low error are shown (PET and TLY) for comparison with two stations that consistently reported biased results (WRAB and PALK). The space-time evaluations show that none of the stations were consistently reporting preferential errors at any locales, nor at time periods that could be attributed to source and path effects, or instrument and configuration changes.

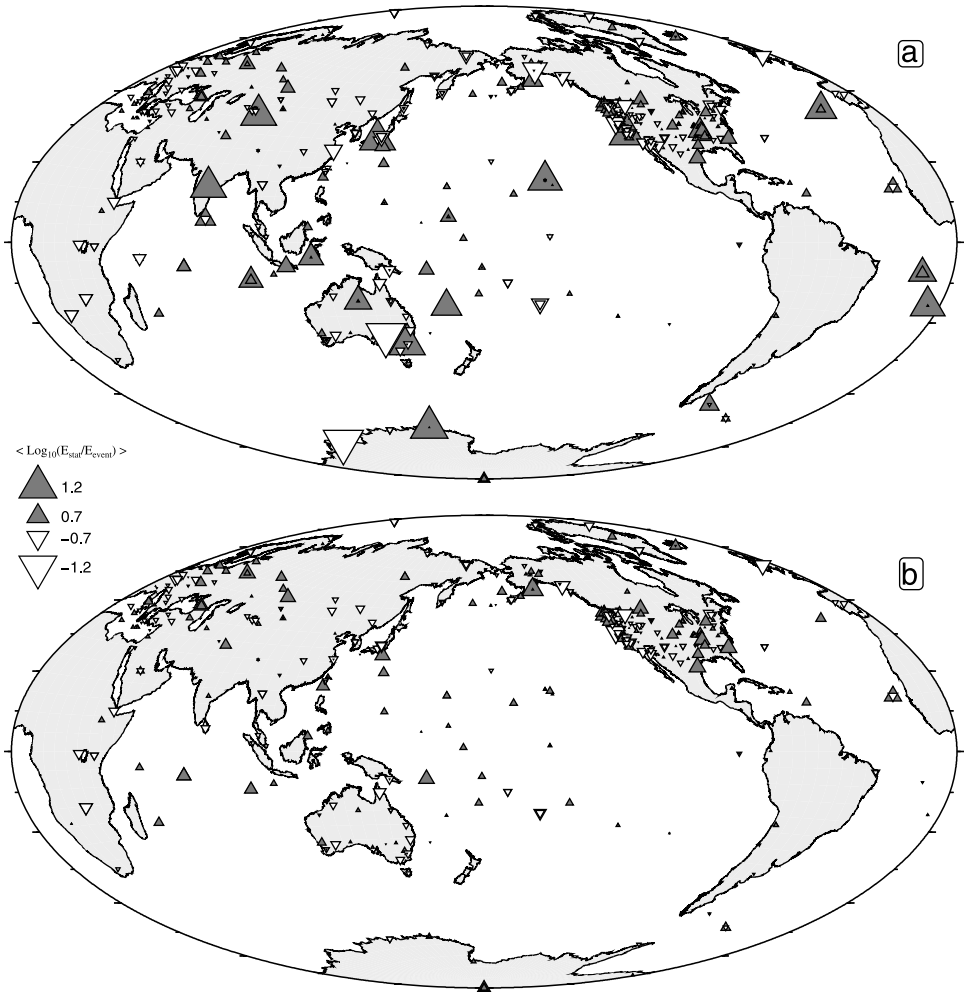

Figure 5. Seismic stations with at least 10 recorded events in the global catalog. The triangle size represents the mean logarithmic deviation the station reports from the determined event mean. The logarithmic deviations are displayed (a) before and (b) after station corrections are applied to the 31 stations that revealed a clear and consistent deviation.

tional energy is much less than the error in energy determination in most results.

2.3. Station Performance and Corrections

[18] As global seismology becomes more data rich, it is easy to be overwhelmed by the ever increasing number of stations that become available. Unfortunately, in some cases the instrument response information may not be properly documented or updated, causing biased determinations of energy. To reduce the effect of this bias and to improve our ability to utilize fewer stations for some real-time applications, we investigate recordings from each station independently, to identify stations that consistently underestimate or overestimate the mean E of recorded events.

[19] Of the 1342 stations used for energy determinations in this study, we examine the 514 stations that were used for 10 or more events. We define a simple per station geometric deviation $\sigma_g^{\pm}$ that retains the sign of the offset as

$$\sigma_g^{\pm} = \log_{10}\left(\frac{E_s}{\bar{E}^*}\right). \quad (3)$$

where E_s and $\bar{E}^*$ are the single-station energy, and the initial mean event energy utilizing all stations. For those 514 stations, we evaluated the azimuthal and temporal behavior. Examples of four stations are shown in Figure 4; two of each accurate, and biased stations.

[20] Of the stations observed, 31 exhibited clear and consistent overestimations or underestimations of radiated energy (Figure 4, and Figure S1 of the auxiliary material). Azimuthal and temporal deviations in energy calculations for stations with 50 or more recorded events are included in Figure S2 of the auxiliary material. Interestingly, none of the stations showed an obvious azimuthal dependence, suggesting that regional variability in crustal attenuation structure was not a major factor in the observed station errors. Additionally, no station was found to have a substantial change in results over time, suggesting no incorrectly or undocumented changes in station instrumentation or parameter files were observed in our study. Likewise, we found no consistent regional biases across the global network (e.g., Figure 5a), and hence regional variations in attenuation do not appear to significantly hamper global calculations. A case example are two stations in south eastern Australia, STKA(AU) and CAN(G), where each have con-

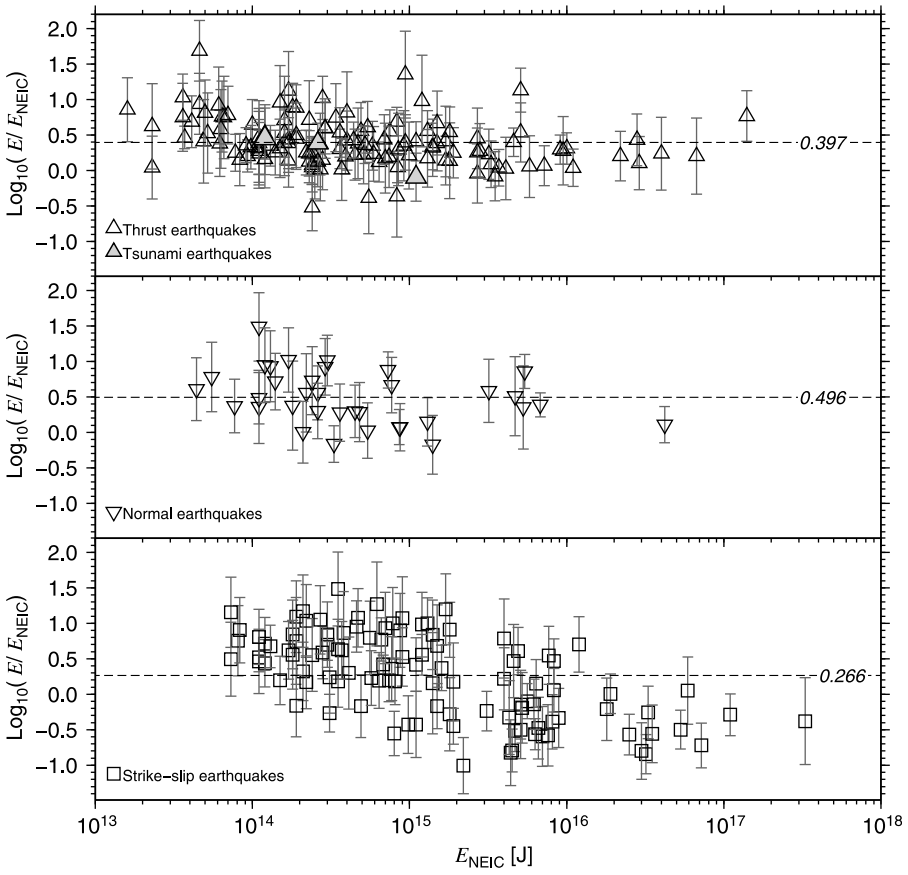

Figure 6. Comparison of energy determinations reported within the National Earthquake Information Center (NEIC) following *Boatwright and Choy* [1986] and this study, and distinguished by faulting mechanism. The error bar lengths correspond to 1σ from this study. Relative to the NEIC results, dip-slip earthquakes in this study are regularly reported to be higher in E, while strike-slip events are more variable.

sistent near order-of-magnitude differences in their average energy determinations from the globally determined results, however, because these are opposite in direction, we conclude that over the period of our observation, deviations such as these appear to be largely due to persistent issues with instrument response files.

[21] For each of the 31 identified stations with permanent deviations, we implemented a station correction based on the value of their mean deviation

$$\bar{\sigma}_g^{\pm} = \left(\frac{\Sigma\sigma_g^{\pm}}{N}\right), \tag{4}$$

where $10^{-\bar{\sigma}_g^{\pm}}$ is the multiplicative factor by which a station's energy would be corrected for a new single-station event energy estimation. The resultant new per station deviation from the new mean energies are shown in Figure 5b. The final per station energy estimates reported in this study are then used to calculate a new mean event energy $\bar{E}$ using the geometric average of all stations (hereafter simply E). We compare our individual event E to those analyzed by the U.S. Geological Survey's National Earthquake Information Center (NEIC, *http://earthquake.usgs.gov/earthquakes/*). Though both results follow *Boatwright and Choy* [1986], the NEIC method uses a modestly different adaptation for windowing and frequency, and generally rely on fewer, and potentially different stations. While results largely agree, there is nearly 1 order of magnitude of scatter, and a modest tendency for relatively smaller reported E for larger earthquakes in this study, particularly for larger strike-slip events (Figure 6).

3. Results

[22] For each of the earthquakes in this study, we compare our determination of E with M_0 obtained from the gCMT catalog to reevaluate the energy-to-moment ratio discriminant θ of *Newman and Okal* [1998], defined as

$$\theta = \log_{10}\left(\frac{E}{M_0}\right). \tag{5}$$

Because of its scale invariance, and the fact that E does not saturate for large earthquakes, a simple conversion from E to an earthquake energy magnitude M_e is possible [*Choy and Boatwright*, 1995]:

$$M_e = \frac{2}{3}\log_{10}(E) - 2.9. \tag{6}$$

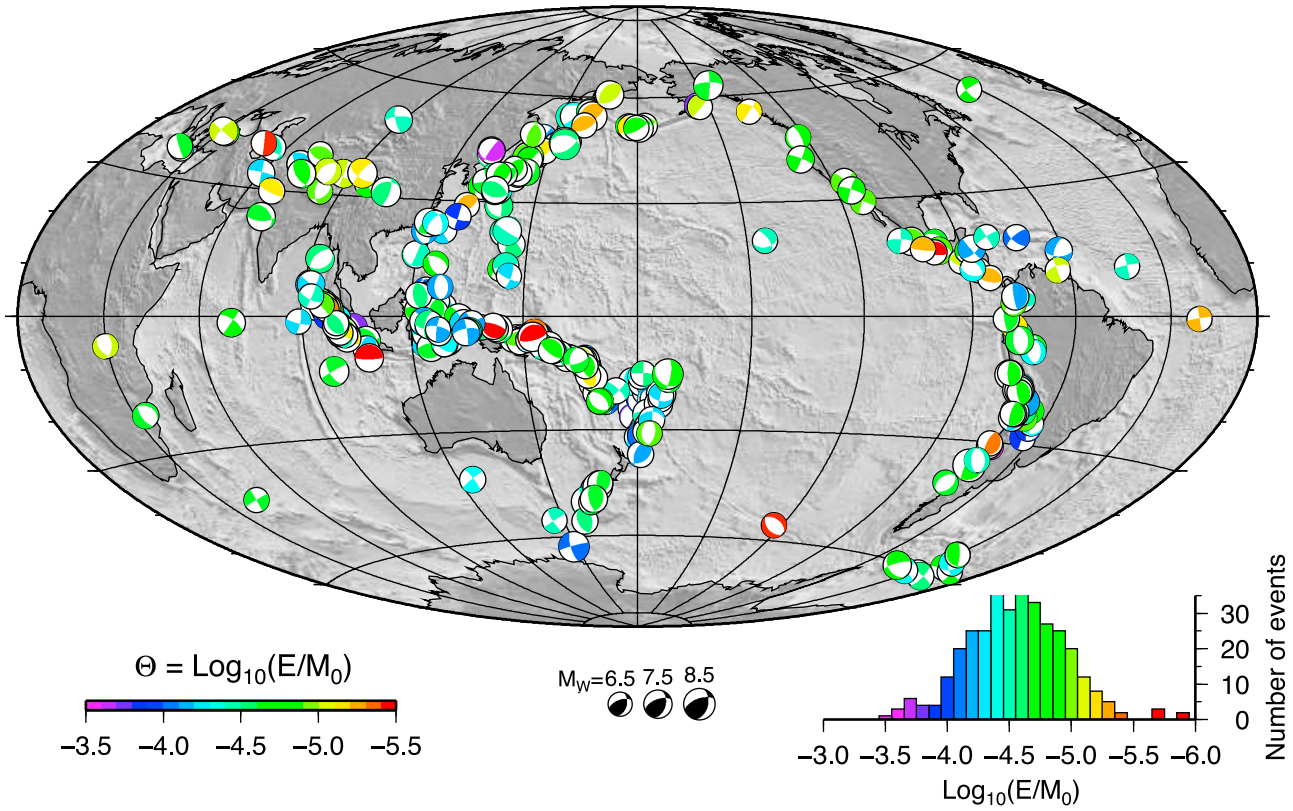

Figure 7. Distribution of focal mechanisms in the global catalog of earthquakes in this study (all recorded events between 1997 and mid-2010 with $M_0 \geq 10^{19}$). Focal mechanisms from the gCMT catalog [*Dziewonski et al.*, 1981; *Dziewonski and Woodhouse*, 1983; *Ekström et al.*, 2005] are plotted with shallower events overlapping deeper ones and colored by their corresponding energy-to-moment ratio. Histogram shows the distribution of θ values plotted in map.

[23] While θ is largely scale-invariant, there is substantial variability within this parameter that emerges when events have relatively stronger or weaker ruptures than their corresponding M_0 would suggest. An important case of these are slow source TsE that are energetically deficient with more than 50% reduction in their rupture velocity [*Newman and Okal*, 1998; *Weinstein and Okal*, 2005; *Newman et al.*, 2011a].

3.1. Global Catalog

[24] The global catalog (Table S1 of the auxiliary material) consists of all large earthquakes with $M_0 \geq 10^{19}$ Nm which occurred between 1997 and mid-2010 as reported within the gCMT catalog (Figure 7). The catalog is composed of 342 events recorded by 17849 seismograms from 1342 stations. As shown in Figure 8, energy determinations scale well with seismic moment, hence no obvious changes in θ are observed over the nearly 4 orders of magnitude of this study. For all events in this study we find the average $\bar{\theta} = -4.59 \pm 0.36$, somewhat higher than previous studies by *Newman and Okal* [1998] and *Weinstein and Okal* [2005] which found −4.98 and −5.12, respectively.

[25] While the energy method works well for most events, there are rare instances when analysis of significantly smaller early aftershocks unrealistically overestimate energies. Two events, an M_W 6.7 event following 26 minutes after the 2006 M_W 8.3 Kuril Islands earthquake, and an M_W 6.9 event that occurred 32 minutes after the 2007 M_W 8.1 Solomon Islands earthquake both reported energies equivalent to an M_e 8.3, due to the overwhelming contribution of main shock surface wave energy at lower frequencies. These events are documented in Table S1 of the auxiliary material and were excluded from all statistical analysis, they are noted here to illustrate the difficulty in determining robust energy calculations for smaller aftershocks immediately following very large earthquakes.

3.1.1. Focal Mechanism

[26] We further evaluate how our calculated value of θ changes with mechanism by subsetting the catalog into thrust (Figure 8b), normal (Figure 8c), and strike-slip (Figure 8d) earthquakes. We find that thrust earthquakes tend to be energetically deficient, having a mean $\bar{\theta}_T = -4.74$, while both normal and strike-slip earthquakes tend to be modestly stronger (or more energetic) than the global average with $\bar{\theta}_N = -4.51$ and $\bar{\theta}_{SS} = -4.44$, respectively. This apparent variation of θ is in agreement with observations of the focal mechanism dependence by *Perez-Campos and Beroza* [2001] and *Choy and Boatwright* [1995]. Applying a Student's t test to each of the subsets [*Press et al.*, 1992], we find that while both thrust and strike-slip earthquakes are distinctly different than each other, and the group average at 99.9% confidence, the remaining normal faulting earthquakes can only be consid-

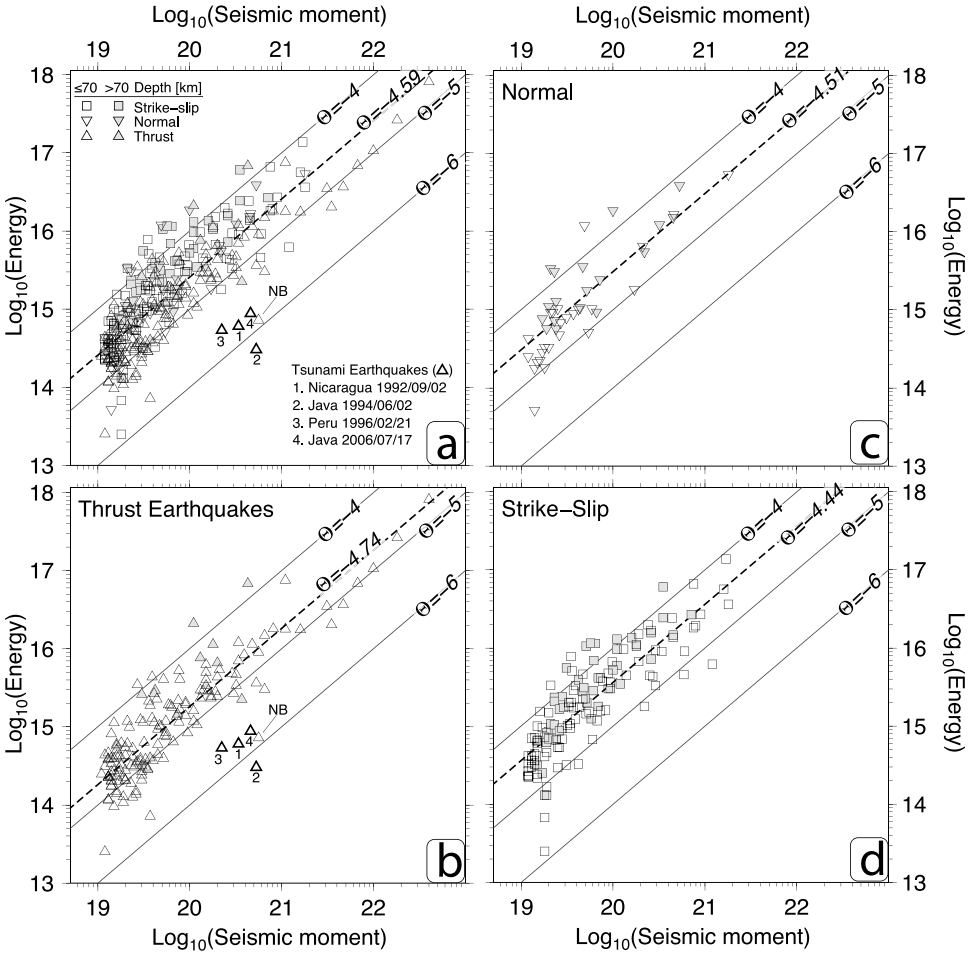

Figure 8. (a) E to M_0 comparison for the global catalog in this study (all events with $M_0 \geq 10^{19}$ between 1997 and mid-2010). Events are identified by their dominant mechanism and illustrated separately as (b) thrust (triangles), (c) normal (inverted triangles), and (d) strike-slip (squares). The dashed line represents the average value of the E/M_0 discriminant θ for each group. Events deeper than 70 km depth (shaded symbols) and TsE (bold triangles) are also differentiated. E deficient earthquakes tend to the bottom right, while strong rupturing events tend to the top left. TsE before 1997 are from A. V. Newman and J. A. Convers (submitted manuscript, 2011) and are included for comparison. Note the energy deficient New Britain earthquake (NB), which is not a known TsE.

ered different than the group average at 80% confidence. Thus, we consider the groups to be distinct, with normal faulting earthquakes being intermediate between thrust and strike-slip events, in energy. We observe no significant moment dependence for any of the focal mechanism subsets: a result that is somewhat surprising given the more than order-of-magnitude downward deviation found when comparing our strike-slip results with those reported by the NEIC (Figure 6).

3.1.2. 2006 Java TsE

[27] Within the subset of thrust events, one known TsE was identified, the 17 July 2006 M_W 7.8 Java earthquake. The event was found to have $\theta = -5.7$, identifying it as a TsE following the discriminant threshold established by *Newman and Okal* [1998] ($\theta_{TsE} \leq -5.7$), and updated utilizing their full rupture duration in the work of A. V. Newman and J. A. Convers (submitted manuscript, 2011) ($\theta_{TsE} \leq -5.6$). This event is shown with the 3 TsE events that occurred in the 1990s for comparison in Figures 8a and 8b.

3.1.3. Slow Source New Britain Earthquake

[28] One event, the 17 November 2000 M_W 7.8 New Britain earthquake, is not known to have caused any tsunami [e.g., *Geist and Parsons*, 2005; *Sahal et al.*, 2010], yet shares several features identified in TsE, including comparable magnitude, long rupture duration ($T_{XO} = 95$ s), shallow depth ($z = 17$ km as reported in the gCMT catalog), and low $\theta = -5.9$. While this earthquake cannot be considered a TsE by its definition of disproportionately large tsunami given by *Kanamori* [1972], it shares the essential characteristics of other slow source TsE events [*Newman and Okal*, 1998; *Polet and Kanamori*, 2000; A. V. Newman and J. A. Convers, submitted manuscript, 2011], and hence we classify the earthquake as simply "slow source". Interestingly, this event was the second major aftershock that followed another M_W 7.8 aftershock (occurring 14 hours earlier) and the November 16 M_W 8.0 main shock, both modestly deficient in energy, with $\theta = -5.3$. A regional tsunami did occur from these events (being recorded as far away as Honiara, Solomon

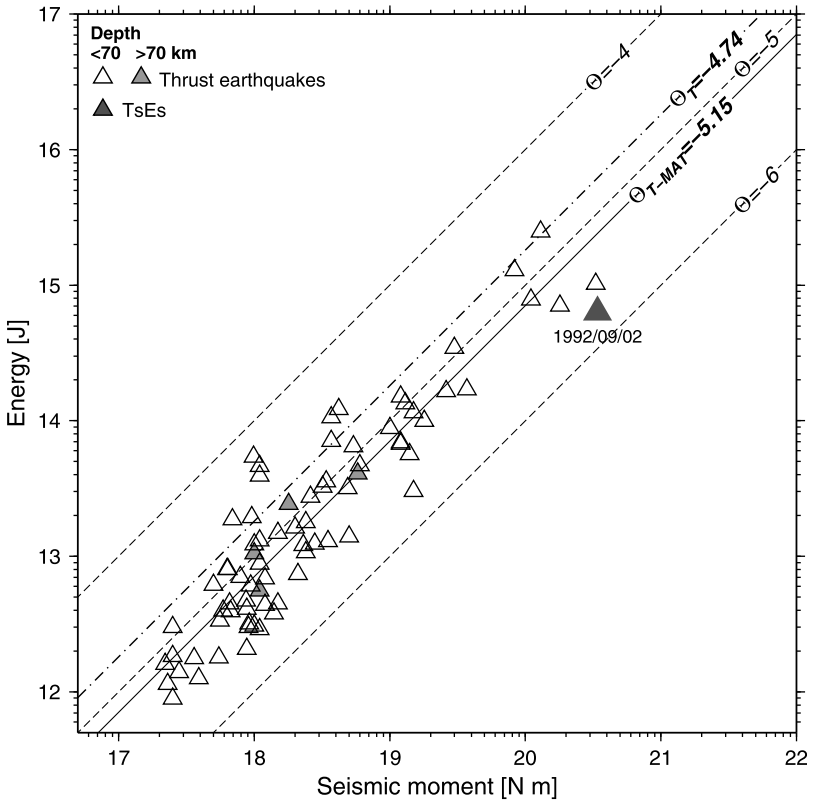

Figure 9. E to M_0 comparison for the Central American thrust events of this and the *Okal and Newman* [2001] studies (similar to Figure 8). The average regional $\bar{\theta}_{T-MAT} = -5.15$ is visibly below the global $\bar{\theta}_T = -4.74$ and does not have a clearly observable moment dependence.

Islands, and Port Vila, Vanuatu), but current evidence supports waves coming from either the main event or its first aftershock which preceded the slow source New Britain event by more than 24 hours [*Geist and Parsons*, 2005]. The discovery of this event's slowness leads to an important implication for real-time TsE warning. Because the current classification of a TsE is dependent on identifying the slow source character of these events, we caution that such tsunami warning methods are susceptible to identifying slow source events that are nontsunamigenic.

3.2. Regional Catalogs

[29] We construct two regional catalogs utilizing the same procedure and time range as the global catalog, but including smaller events ($M_0 \geq 2 \times 10^{17}$ Nm, $M_W \geq 5.5$). The regions selected include the subduction zones along the Middle America and Java trenches, both of which recorded recent TsEs; the 2 September 1992 M_W 7.7 earthquake offshore Nicaragua [*Ide et al.*, 1993; *Inamura et al.*, 1993], and the 2 June 1994 M_W 7.8 and the 17 July 2006 M_W 7.7 earthquakes offshore Java [*Abercrombie et al.*, 2001; *Ammon et al.*, 2006]. To determine if the subduction megathrusts in these environments are particularly susceptible to slow rupturing events, we evaluate only the thrust earthquakes that occur in each region with gCMT depths less than 70 km. For each region, the data sets are complemented by thrust events above $M_0 \geq 5 \times 10^{17}$ Nm ($M_W \geq 5.7$), recorded between 1981 and 1997 by *Okal and Newman* [2001].

3.2.1. Middle America Trench

[30] Along the Middle America Trench (MAT), we determined the radiated seismic energy for 53 thrust events, and compared with those reported by *Okal and Newman* [2001] (Figure 9 and Table S3 of the auxiliary material). From the two studies, the combined energy-to-moment discriminant results for thrust events along the MAT is $\bar{\theta}_{T-MAT} = -5.15$, one-third of global thrust average value (Figure 10). Using data from this study alone, we find $\bar{\theta}_{T-MAT} = -5.1$, modestly higher than observed in thrust events reported only in the study by *Newman and Okal* [1998], $\bar{\theta}_{T-MAT} = -5.2$. Changes in θ between the data sets occur, in part, due to the improved event-dependent time window used for energy determinations in this study. On average, energy determinations should be modestly reduced because calculations in this study are run to T_{XO}. For most events, this value is less than the default window of 70 s used in the previous analysis by *Okal and Newman* [2001]. However, the 1992 TsE had $T_{XO} = 165$ s and yielded $E = 6.1e14$ J, almost 2.4× larger than the E (2.5e14 J) reported by *Newman and Okal* [1998] using only a 70 s window. The significant increase in energy caused by using the event-dependent duration yields $\theta = -5.7$, which is less energetically deficient than previously reported (old $\theta = 6.1$) [*Newman and Okal*, 1998]. The energy increase is roughly equivalent to the extended duration of determination, because radiated energy growth is observed to be near constant for slow and other long-duration earthquakes [*Weinstein and Okal*, 2005; *Newman et al.*, 2011a]; see Figure 2 as an example.

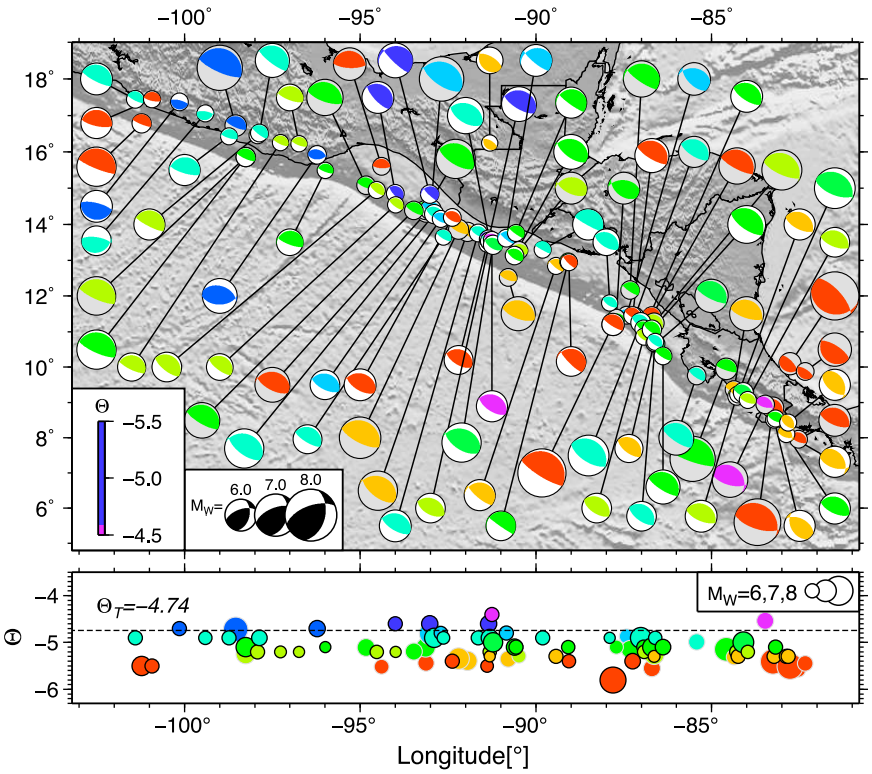

Figure 10. Central American thrust events (gCMT epicenters and solutions) occurring primarily along the Middle America Trench (MAT) are shown for this study (49 events between 1997 to mid-2010, white P quadrants) and from *Okal and Newman* [2001] (28 events between 1981 to 1997, gray P quadrants). The focal mechanisms are colored corresponding to the energy-to-moment parameter θ. The longitudinal variations in θ highlight the overall low energy ruptures in the region with almost all earthquakes being more energy deficient than the global thrust average of $\theta_T = -4.74$ (dashed line).

[31] Almost all thrust events along the MAT are deficient in radiated E compared to the global thrust average of $\theta = -4.74$ (Figures 9 and 10). With the exception of one event from the *Okal and Newman* [2001] catalog, all earthquakes examined off of Nicaragua and Costa Rica (East of 90°W, Figure 9) are below the average. Events occurring further to the northwest are mostly reduced in θ, but include more energetic events. Clearly, Central American thrust earthquakes are energetically deficient relative to the global data set.

[32] To evaluate whether the observed increase in source rupture speed with depth identified by *Bilek and Lay* [1999] yields a comparable increase in θ, we compare E to both hypocentral and gCMT depth determinations. While the former gives more precise information of the event initiation, the latter is a better descriptor of the mean depth by which most of the moment release occurs. The hypocentral solutions come from the EHB catalog when available [*International Seismological Centre*, 2009], otherwise defaulting to depths reported by the NEIC Bulletin.

[33] For events along the MAT, we find an increase in θ with increasing gCMT depth but with large scatter (Figure 11, left). The trend becomes less clear when examining merely hypocentral depths (Figure 11, right). For events that dominantly slip in the shallow megathrust environment (gCMT depth $\leq$ 20 km), θ is consistently low and below the global thrust average. In contrast, as depth increases, earthquakes tend to have relatively larger values of θ, with events at gCMT depth greater than 40 km having θ close to the global average. The best linear trend of the variability of θ with depth $z(\theta)$ yields a slope of 3.4 ± 8.6 km/θ and intercept of a = 59 ± 44 km (Figure 11), however, the fit is highly scattered, and any interpretation of the fit should be limited.

3.2.2. Java Trench

[34] We similarly analyze the Java trench, the only source known to have two TsE since the development of the global seismic network. We performed energy determinations for 34 thrust events, and compared them to the 7 available from the *Okal and Newman* [2001] study (Figure 12 and Table S4 of the auxiliary material). Unlike the results from the Central American study region, the thrust events here have average energy ratios $\bar{\theta}_{T-JV} = -4.91$, statistically equivalent to the global thrust average $\bar{\theta}_T = -4.74$ (Figure 13). Little difference is observed between the thrust events in this study and the one obtained by *Okal and Newman* [2001], with the two having similar mean values $\bar{\theta}_T = -4.9$ and -5.0, respectively. However, the inclusion of nearly fivefold the data allows for a more robust evaluation of the depth dependence of θ.

[35] Though the average of thrust events near Java are close to the global average, unlike Central America, the events show a more robust depth dependence when using the gCMT reported values (Figure 14). Shallow earthquakes are highly scattered between the energetically deficient TsE events with

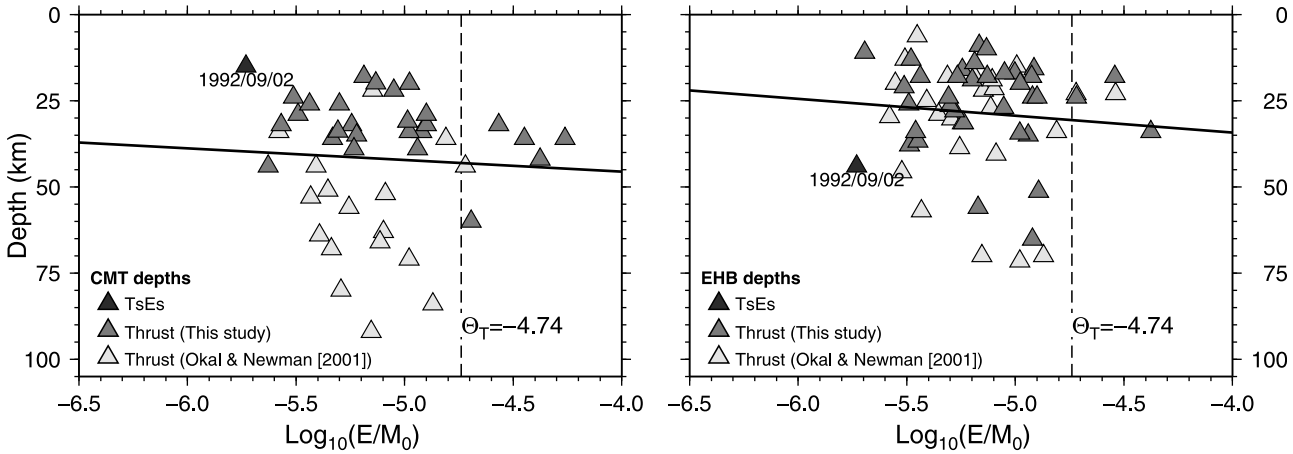

Figure 11. The same Central American events from Figures 9 and 10 shown as a function of (left) gCMT and (right) hypocentral depth and θ ($\mathrm{Log}_{10}(E/M_0)$). EHB depths were used when available [*International Seismological Centre*, 2009], otherwise depths are from the NEIC. Events are observed to be depth-dependent and split into two groups. The linear trend (solid line) described events determined in this study (dark triangles) with linear fits using the gCMT depths (intercept 59 ± 44 km, and slope 3.37 ± 8.5 km/θ), and the EHB depths (intercept of 53.6 ± 36 km and slope 4.86 ± 7 km/θ).

$\theta < -5.7$ and energetic events with $\theta > -4.5$, but there is a trend where as depth increases, the values of θ become comparable to the global average. The distribution here is bifurcated with two trends; one of an apparent constant steeper gradient, and another showing a range of shallow earthquakes with higher values of θ that occur primarily in the Flores Sea region. Removing events from this region (Latitude ≥ −9°, Longitude ≥ 115°), we find an apparent linear trend for $z(\theta)$ of increased θ with gCMT depth, where the slope is 25.8 ± 6.2 km/θ and intercept 171 ± 31 km.

4. Discussion

[36] In evaluating the relative energy release with earthquake size in this study we find a mean energy-to-moment ratio $\bar{\theta} = -4.59$, similar to the scale-invariant solution $\theta =$

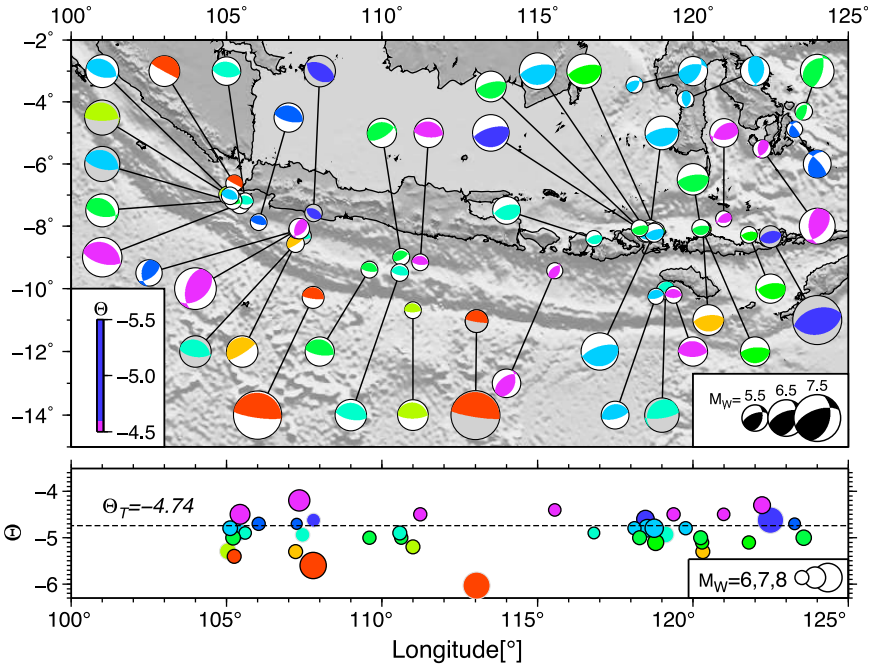

Figure 12. (top) Focal mechanisms for Java thrust earthquakes are shown for this study using the gCMT focal solutions and epicenters (34 events between 1997 to mid-2010, white P quadrants) and from *Okal and Newman* [2001] (7 events between 1981 to 1997, gray P quadrants); similar to Figure 10. (bottom) No longitudinal variation is apparent, with most seismicity having θ near the global thrust average of $\theta_T = -4.74$ (dashed line).

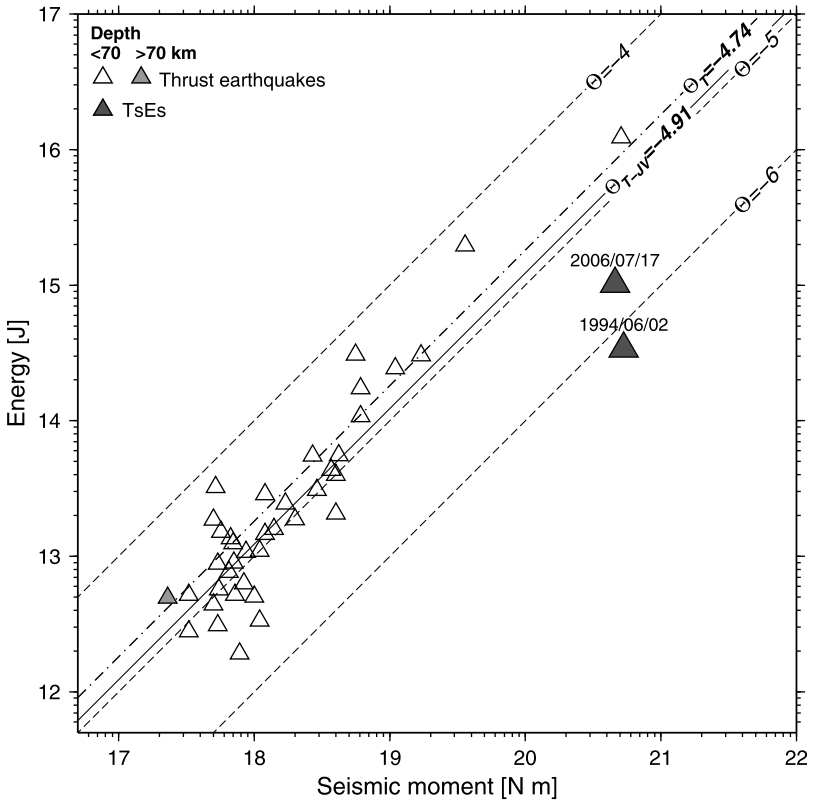

Figure 13. E to M_0 comparison for Java thrust events of this and the *Okal and Newman* [2001] studies (similar to Figures 8 and 9). The average regional $\theta_{T-JV} = -4.91$ is comparable to the global $\theta_T = -4.74$, reduced mostly by the occurrence of the two known TsEs.

−4.5 that was identified between 3×10^3 to 2×10^{21} Nm [*Ide and Beroza*, 2001]. Because of the recent occurrence of giant earthquakes in Sumatra and Chile, we can extend that range to 4×10^{22} Nm, yielding now 19 orders of magnitude of scale invariance.

[37] This study finds higher energy-to-moment results than that of *Newman and Okal* [1998], with $\bar{\theta} = -5.0$. The difference between the two studies occur from the inclusion of (1) the full rupture duration; (2) deep earthquakes (depth ≥ 70 km); and (3) events from different time periods. The first

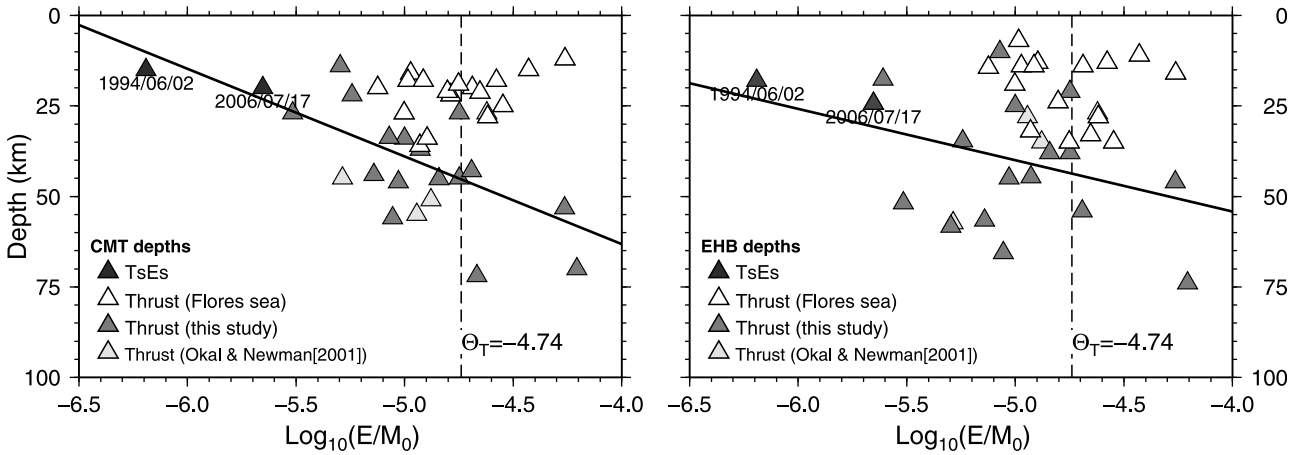

Figure 14. The same Java events from Figures 12 and 13 shown as a function of (left) gCMT and (right) hypocentral depth and θ ($\mathrm{Log}_{10}(E/M_0)$). EHB depths were used when available [*International Seismological Centre*, 2009], otherwise depths are from the NEIC. When excluding events within the Flores Sea (lat ≥ −9°, longitude ≥ 115°; open triangles), a depth-dependent trend $z(\theta)$ is apparent from the gCMT depths with intercept 171 ± 31 km, and a slope of 25.8 ± 6 km/θ following a linear fit. Note some events are deeper than the depth cutoff (70 km) based on gCMT reports.

two differences have the effect of increasing the determinations of energy. Utilizing the full rupture duration captures the additional radiated energy in very large earthquakes (50 events with $T_{XO} > 70$ s in this study) that would not be measured at the 70 s cutoff of *Newman and Okal* [1998]. Most notably, the Sumatra 2004 earthquake has less than 15% of the total radiated energy in the first 70 s of its 540 s T_{XO} determined rupture. Additionally, because TsE events all have $T_{XO} > 70$ s, their full radiated energy would otherwise be lost. Reevaluation of θ as a discriminant for TsE events finds that when utilizing the full duration of rupture, a modestly lower value of $\theta_{TsE} \leq -5.6$ is necessary (A. V. Newman and J. A. Convers, submitted manuscript, 2011), rather than $\theta_{TsE} \leq -5.7$ found by *Newman and Okal* [1998]. The addition of 70 deep earthquakes (depth > 70 km) in this study increases the global average values because these events rupture with higher relative radiated energies ($\bar{\theta}_{deep} = -4.32$). The last major difference between the two analysis is the inclusion of more events (342 events here vs. 52 events in the work of *Newman and Okal* [1998]), most of these with significantly more available data. On average, more than 50 stations are used per determination in this study, as compared to only 10 in the earlier analysis by *Okal and Newman* [2001]. This, and the additional careful correction of 31 stations that yielded biased solutions, allow for improved E determinations for individual events, as well as the global average.

[38] A direct physical interpretation of E/M_0 or θ is somewhat difficult since the ratio can be combined to approximate several parameters, when others are held constant. Most fundamentally, the ratio is a relationship between the dynamically radiated energy E and the amount of work done to cause the fault to slip, represented by M_0 [e.g., *Kanamori and Rivera*, 2006].

[39] Assuming an earthquake is perfectly efficient at radiating energy (i.e. no work goes into tearing or heating the fault) the energy-to-moment ratio can be directly related to dynamic stress drop $\Delta\sigma$:

$$\Delta\sigma = 2G\left(\frac{E}{M_0}\right), \tag{7}$$

where G is the near-source crustal rigidity [*Hanks and Kanamori*, 1979; *Stein and Wysession*, 2003].

[40] Alternatively, the radiated seismic efficiency η_R is useful for evaluating the relative speed (or 'snappiness') of earthquake rupture, given that the static stress drop $\Delta\sigma_s$ is assumed constant. *Husseini and Randall* [1976] first characterized the parameter as

$$\eta_R = \left(\frac{2G}{\Delta\sigma_s}\right)\left(\frac{E}{M_0}\right). \tag{8}$$

[41] The radiated efficiency varies almost uniformly between 0 and 1 with the ratio of the rupture velocity V_R and the rupture limiting speed (usually the shear wave speed) [*Kanamori and Rivera*, 2006], and hence an earthquake that ruptures more/less rapidly would have increased/decreased radiation efficiency and θ parameter. Because an inherent trade-off exists between η_R and $\Delta\sigma_s$, which is not independently evaluated here, we prefer to characterize θ in terms of a third parameter, apparent stress τ_a. *Wyss and Brune* [1968] originally described τ_a as the product of the energy-to-moment ratio and rigidity. By assuming dynamic and static stress drop are roughly equivalent, this relation can be directly linked with η_R through

$$\tau_a = G\left(\frac{E}{M_0}\right) = \frac{\eta_R \Delta\sigma}{2}. \tag{9}$$

[42] While describing the energy-to-moment ratio in terms of radiation efficiency is useful for events like slow-rupturing TsE that are limited by V_R, it may not be optimal as a generic characterization for global earthquake activity. Thus, we more generically describe E/M_0 in terms of τ_a which requires only an assumption of G.

4.1. Mechanism Dependence

[43] On average, strike-slip earthquakes are more energetic, having $\bar{\theta}_{SS} = -4.44$, higher than the global average (Figure 8b). While small, this difference is robust, and is suggested to stem from the rupture of strong lithosphere along the edges of oceanic transforms, or intraplate environments, both are observed to have increased $\Delta\sigma$ or τ_a [*Schorlemmer et al.*, 2005; *Allmann and Shearer*, 2009; *Feng et al.*, 2010; *Choy and McGarr*, 2002; *Choy et al.*, 2006]. This is in contrast to thrust mechanisms that are generally less energetic, having $\bar{\theta}_T = -4.74$, corresponding to an approximate 30% reduction in τ_a. Though also occurring in intraplate regions, they occur dominantly along subduction megathrusts, the environments responsible for excessively energy deficient TsE events [*Newman and Okal*, 1998; *Polet and Kanamori*, 2000; A. V. Newman and J. A. Convers, submitted manuscript, 2011]. In this study, we find normal faulting earthquakes to be intermediate between the other mechanisms, and not distinguishable from the global average. This is analogous to results obtained for apparent stress, that also locate normal earthquakes between thrust and strike-slip earthquakes [*Choy and Boatwright*, 1995]. The relative higher value of $\theta_N = -4.51$, compared to thrust earthquakes, has been related mostly to slip on immature faults, such as those in cold and intact lithosphere [*Choy and Kirby*, 2004].

4.2. Depth Dependence

[44] Examination of $\Delta\sigma$ or τ_a with various focal mechanisms and at different depths has been done for different magnitude ranges and settings, identifying the largest values for strike-slip earthquakes [e.g., *Choy and Boatwright*, 1995; *Perez-Campos and Beroza*, 2001; *Venkataraman and Kanamori*, 2004; *Choy et al.*, 2006; *Allmann and Shearer*, 2009]. While higher values are found in strike-slip environments and lowest for reverse faulting earthquakes, a clear characterization of the depth dependence of τ_a remains problematic. *Allmann and Shearer* [2009] find a median $\tau_a = 2$ MPa (converted from $\Delta\sigma = 4$ MPa), with slight but nonconclusive depth dependence. As well, *Venkataraman and Kanamori* [2004] were unable to find a clear depth dependence in a global evaluation of earthquakes shallower than 100 km depth. The lack of a clear trend in these studies are in contrast to our results for regional and global thrust earthquakes (Figures 11, 14, and 15), as well as those expected from the study of *Bilek and Lay* [1999], which attributed a depth dependent change in source durations due to a reduction of rigidity in shallow subduction environments, possibly caused by lesser sediment compaction. Decreasing rigidity potentially affects the rupture

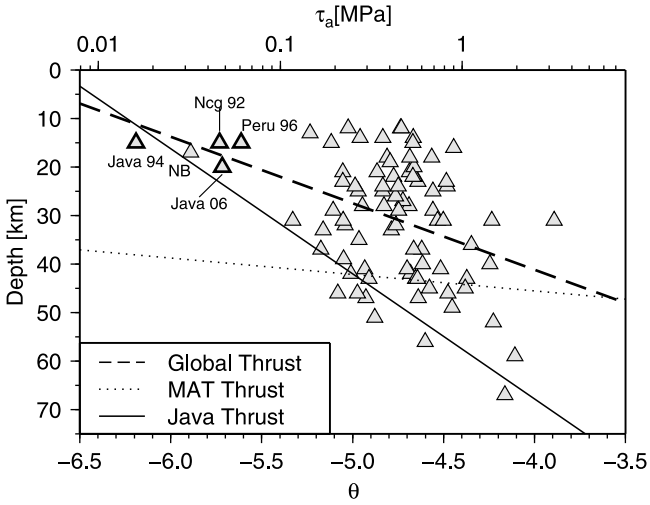

Figure 15. The gCMT depth dependence of global thrust earthquakes is shown relative to θ and its conversion to apparent stress τ_a using equation (9). While steeper than the global distribution (dashed line; linear fit with intercept 95.9 ± 21 km and slope 13.7 ± 4 km/θ), the trend determined from the Java thrust earthquakes (solid line; Figure 14, left) is considered more representative of subduction zone behavior, as the global thrust catalog contains results from intraplate environments. The trend for the Middle America Trench (MAT; dotted line) is also shown for completeness. The five slow source earthquakes, comprising the four observed TsE events and the 2000 New Britain (NB) earthquake, all roughly follow this trend.

velocity, and consequently the overall rupture duration [*Bilek*, 2007; *Houston*, 2001; *Vidale and Houston*, 1993]. Alternatively, assuming no change in regional rigidity, the depth-dependent change in energy-to-moment ratio can be attributed to a change in τ_a due to increased lithostatic pressure.

[45] There is large scatter in our observed depth dependence of θ, with activity along the Java trench being highly dependent, compared to the moderate behavior of the MAT (Figure 15). While some shallow events that have relatively higher θ values (and τ_a) may represent intraplate crustal activity on immature faults, others can likely be attributed to complexities along the fault interface.

[46] Conversion of θ to τ_a for subduction thrust earthquakes shows a linearly trending minimum θ envelope with depth, where τ_a increases from about 15 kPa near the trench to about 2 MPa near 70 km depth (Figure 15). Assuming $\tau_a = \Delta\sigma/2$, this result is comparable to the depth-$\Delta\sigma$ relationship of *Bilek and Lay* [1999], which was found assuming constant rupture velocity. Events deeper than 70 km likely occur within the slab, and hence may represent immature fault behavior. Thus, our high θ values for these events is expected ($\bar{\theta}_{deep} = -4.32$).

[47] A limitation in this generalized study is that we utilize a frequency-dependent attenuation correction that is not depth-dependent [*Choy and Boatwright*, 1995]. Such a correction, will overestimate the attenuation from the direct *P* wave, while underestimating the contribution from *sP* and *pP*. We use this because a more complex depth-dependent attenuation would need to adequately account for the focal mechanism-dependent contribution of the depth phases which are preferentially attenuated along the source side crust; a region avoided by the direct *P* wave in deep earthquakes.

4.3. Regional Results

[48] While analysis of the Java trench yields no consistent energy deficiency (Figure 12), with most events occurring very near the global average thrusting $\bar{\theta}_T$, thrust events along the MAT were consistently deficient in *E* (Figure 9). The regional average across the MAT is $\bar{\theta}_{T-MAT} = -5.15$, about one-third the global thrust average and is consistent with other studies that have found low stress drop in the region [*Allmann and Shearer*, 2009; *Eissler et al.*, 1986; *Iglesias et al.*, 2003]. Interestingly, the negative deviation from the global thrust average appears to change linearly along-strike of the trench, becoming increasingly negative toward the southeast section. At the southeastern terminus of the regional study, near the Costa Rica-Panama border, (located toward the lower right region of map in Figure 10), θ values are most reduced, including events both along the MAT and along shallow thrusts along the back arc. At this locale the failed Cocos ridge subducts [e.g., *Protti et al.*, 1994], potentially increasing local high-frequency attenuation. Alternatively, because the rate of convergence gradually increases to the southeast from 70 to approximately 100 mm yr^{-1} [*DeMets*, 2001], there may be a modest increase in fault maturity due to increased cumulative slip, thus allowing for reduced τ_a [*Choy and Kirby*, 2004; *Schorlemmer et al.*, 2005; *Choy and Boatwright*, 2009].

[49] When excluding events that occur northeast of the islands of Java (those mostly associated with subduction in the Flores Sea), we find that thrusts have a strong gCMT depth dependence, with increasingly deep events being more energetic (Figure 14). This trend of increased θ with depth closely follows the trend observed for global thrust mechanisms (Figure 15).

4.4. Real-Time Adaptation

[50] In order to obtain reliable *E* determinations for real-time use, it is necessary to estimate the focal correction for the *P* wave group (F^{gP} in equation (2)) by making assumptions about the orientation of the focal mechanism. While depth is also poorly known initially, it is observed to have little dependence on the final result, only affecting estimated *E* (E_{est}, Table S1 of the auxiliary material) by less than 10% for shallow earthquakes (depth ≤ 70 km) [*Newman and Okal*, 1998]. To correct for focal mechanism, *Newman and Okal* [1998] evaluated the global distribution of gCMT focal mechanisms using existing and available seismic stations to determine a general distant-dependent correction for dip-slip earthquakes. This was chosen over a stochastically distributed event-station correction because the spatial occurrence of focal mechanism orientations is clearly not random.

[51] The use of this generalized radiation coefficient on strike-slip earthquakes will underestimate the true event energy by a factor of four or more, due to the increasingly near-vertical takeoff occurring near the nodal axis of the source focal mechanism at greater teleseismic distances [*Newman and Okal*, 1998; *Perez-Campos and Beroza*, 2001; *Choy and McGarr*, 2002]. Fortunately, less than 15% of all large earthquakes ($M_W \geq 7$) are strike-slip. Improvements to this method could be made by utilizing station and source region specific corrections.

[52] Real-time energies are routinely calculated for all earthquakes of $M_W \geq 6.5$ following the above methodology and reported online (*http://geophysics.eas.gatech.edu/Rterg/*) (A. V. Newman and J. A. Convers, submitted manuscript, 2011). In the case of the 2010 $M_W = 7.8$ Mentawai slow source TsE, the real-time energy is found to be extremely deficient ($\theta = -5.9$), and comparable to other slow source TsE events [*Newman et al.*, 2011a]. In contrast, the real-time evaluation of a smaller tsunamigenic $M_W = 7.1$ 2010 Solomon Islands earthquake was found to have near average energy release ($\theta = -4.8$), and hence unlikely to be slow source in nature [*Newman et al.*, 2011b].

[53] To obtain more rapid estimates, it is possible to rely on stations, particularly low gain, closer than the 25° cutoff used here. However, because of the potential for triplication and biasing from local attenuation structure, results should be handled with extra care. Duration determinations for TsE and very large earthquakes will become increasingly problematic since the $S - P$ time will reduce below 260 s at stations nearer than 25°.

5. Conclusions

[54] The updated global catalog of radiated seismic energy from recent large earthquakes ($M_0 \geq 10^{19}$ Nm) is developed for 342 events using 17849 seismograms. Comparison of the E determinations of this study finds that the radiated seismic energy parameter θ is significantly higher ($\bar{\theta} = -4.59 \pm 0.36$) than previously reported by *Newman and Okal* [1998] and *Weinstein and Okal* [2005] (−4.98, and −5.12, respectively). Utilizing the full duration of the event rupture significantly improves the estimation of very large and slow rupturing events such as giant and tsunami earthquakes. Because of the inclusion of recent giant earthquakes, we now extend the scale-invariant range of $\theta = -4.5$ over 19 orders of magnitude, from 3×10^3 to 4×10^{22} Nm by augmenting the study of *Ide and Beroza* [2001] with events beyond 2×10^{21} Nm.

[55] Similar to previous studies, we observe a robust variation of θ with focal mechanism, as thrust, strike-slip, and normal earthquakes exhibit $\bar{\theta}_T = -4.74$, $\bar{\theta}_{SS} = -4.44$, and $\bar{\theta}_N = -4.51$, respectively. The deficiency in radiated seismic energy in thrust events is potentially due to the preferential occurrence of these events on mature subduction megathrusts [*Choy and Kirby*, 2004], while increased relative radiated energy in strike-slip events likely occur because of their preferential occurrence on immature continental and oceanic transforms.

[56] Regional analyses of thrust events along the MAT and Java trench environments yield mixed results. While Java does not exhibit a preferentially deficient nature, the MAT thrust events are almost exclusively deficient in energy, representing an approximate 30% reduction in τ_a. However, only the Java trench environment exhibits a significant increase in θ with depth down to 70 km, that can be described as a gradual increase in earthquake τ_a from near 15 kPa near the trench to 2 MPa near 70 km depth. The five slow source earthquakes, comprising the 4 observed TsE events and the 2000 New Britain earthquake, are the most energetically deficient end-members of this trend.

[57] **Acknowledgments.** We thank Alicia Nobles for helping to collect and processes seismic waveforms. The efforts made by two anonymous reviewers were substantial and greatly improved the final manuscript. Algorithms used were partially funded through USGS-NEHRP grant 08HQGR0028. NSF grant 0847382 contributed to student and PI effort in support of this project.

References

Abercrombie, R., M. Antolik, K. Felzer, and G. Ekstrom (2001), The 1994 Java tsunami earthquake: Slip over a subducting seamount, *J. Geophys. Res.*, *106*, 6595–6607.

Aki, K., and P. G. Richards (1980), *Quantitative Seismology: Theory and Methods*, W. H. Freeman, San Francisco, Calif.

Allmann, B. P., and P. M. Shearer (2009), Global variations of stress drop for moderate to large earthquakes, *J. Geophys. Res.*, *114*, B01310, doi:10.1029/2008JB005821.

Ammon, C. J., et al. (2005), Rupture process of the 2004 Sumatra-Andaman earthquake, *Science*, *308*(5725), 1133–1139, doi:10.1126/science.1112260.

Ammon, C. J., H. Kanamori, T. Lay, and A. A. Velasco (2006), The 17 July 2006 Java tsunami earthquake, *Geophys. Res. Lett.*, *33*, L24308, doi:10.1029/2006GL028005.

Beresnev, I. A. (2009), The reality of the scaling law of earthquake-source spectra?, *J. Seismol.*, *13*(4), 433–436, doi:10.1007/s10950-008-9136-9.

Bilek, S. L. (2007), Using earthquake source durations along the Sumatra-Andaman subduction system to examine fault-zone variations, *Bull. Seismol. Soc. Am.*, *97*, S62–S70, doi:10.1785/0120050622.

Bilek, S. L., and T. Lay (1999), Rigidity variations with depth along interpolate megathrust faults in subduction zones, *Nature*, *400*, 443–446.

Boatwright, J., and G. Choy (1986), Teleeseismic estimates of energy radiated by shallow earthquakes, *J. Geophys. Res.*, *91*, 2095–2112.

Boatwright, J., and J. Fletcher (1984), The partition of radiated energy between *P* and *S* waves, *Bull. Seismol. Soc. Am.*, *74*, 361–376.

Choy, G., and J. Boatwright (1995), Global patterns of radiated seismic energy and apparent stress, *J. Geophys. Res.*, *91*, 18,205–18,228.

Choy, G. L., and J. Boatwright (2009), Differential energy radiation from two earthquakes in Japan with identical M_w: The Kyushu 1996 and Tottori 2000 earthquakes, *Bull. Seismol. Soc. Am.*, *99*, 1815–1826, doi:10.1785/0120080078.

Choy, G. L., and S. H. Kirby (2004), Apparent stress, fault maturity and seismic hazard for normal-fault earthquakes at subduction zones, *Geophys. J. Int.*, *159*(3), 991–1012, doi:10.1111/j.1365-246X.2004.02449.x.

Choy, G. L., and A. McGarr (2002), Strike-slip earthquakes in the oceanic lithosphere: Observations of exceptionally high apparent stress, *Geophys. J. Int.*, *150*(2), 506–523.

Choy, G., A. McGarr, S. Kirby, and J. Boatwright (2006), An overview of the global variability in radiated energy and apparent stress, in *Earthquakes: Radiated Energy and the Physics of Faulting*, *Geophys. Monogr. Ser.*, vol. 170, edited by R. Abercrombie, A. McGarr, H. Kanamori, and G. Di Toro, pp. 43–57, AGU, Washington, D. C.

DeMets, C. (2001), A new estimate for present-day Cocos-Caribbean plate motion: Implications for slip along the Central American volcanic arc, *Geophys. Res. Lett.*, *28*, 4043–4046.

Der, Z., T. Mcelfresh, and A. Odonnell (1982), An investigation of the regional variations and frequency-dependence of anelastic attenuation in the mantle under the united-states in the 0.5-4hz band, *Geophys. J. R. Astron. Soc.*, *69*(1), 67–99.

Dziewonski, A., and J. Woodhouse (1983), An experiment in systematic study of global seismicity: Centroid-moment tensor solutions for 201 moderate and large earthquakes of 1981, *J. Geophys. Res.*, *88*, 3247–3271.

Dziewonski, A., T. Chou, and J. Woodhouse (1981), Determination of earthquake source parameters from waveform data for studies of global and regional seismicity, *J. Geophys. Res.*, *86*, 2825–2852.

Eissler, H., L. Astiz, and H. Kanamori (1986), Tectonic setting and source parameters of the september 19, 1985 Michoacan, Mexico earthquake, *Geophys. Res. Lett.*, *13*, 569–572.

Ekström, G., A. Dziewonski, N. Maternovskaya, and M. Nettles (2005), Global seismicity of 2003: Centroid-moment-tensor solutions for 1087 earthquakes, *Phys. Earth Planet. Inter.*, *148*, 327–351, doi:10.1016/j.pepi.2004.09.006.

Feng, L., A. V. Newman, G. T. Farmer, P. Psimoulis, and S. C. Stiros (2010), Energetic rupture, coseismic and post-seismic respoonse of the 2008 M_W 6.4 Achaia-Elia earthquake in northwestern Peloponnese, Greece: An indicator of an immature transform fault zone, *Geophys. J. Int.*, *183*, 103–110.

Geist, E., and T. Parsons (2005), Triggering of tsunamigenic aftershocks from large strike-slip earthquakes: Analysis of the November 2000 New Ireland earthquake sequence, *Geochem. Geophys. Geosyst.*, *6*, Q10005, doi:10.1029/2005GC000935.

Hanks, T., and H. Kanamori (1979), A moment magnitude scale, *J. Geophys. Res.*, *84*, 2348–2350.

Houston, H. (2001), Influence of depth, focal mechanism, and tectonic setting on the shape and duration of earthquake source time functions, *J. Geophys. Res.*, *106*, 11,137–11,150.

Husseini, M. I., and M. J. Randall (1976), Rupture velocity and radiation efficiency, *Bull. Seismol. Soc. Am.*, *66*, 1173–1187.

Ide, S., and G. C. Beroza (2001), Does apparent stress vary with earthquake size?, *Geophys. Res. Lett.*, *28*, 3349–3352.

Ide, S., F. Imamura, Y. Yoshida, and K. Abe (1993), Source characteristics of the Nicaraguan tsunami earthquake of September 2, 1992, *Geophys. Res. Lett.*, *20*, 863–866.

Iglesias, A., S. K. Singh, J. F. Pacheco, L. Alcantara, M. Ortiz, and M. Ordaz (2003), Near-trench Mexican earthquakes have anomalously low peak accelerations, *Bull. Seismol. Soc. Am.*, *93*, 953–959.

Inamura, F., N. Shuto, S. Ide, Y. Yoshida, and K. Abe (1993), Estimate of the tsunami source of the 1992 Nicaraguan earthquake from tsunami data, *Geophys. Res. Lett.*, *20*, 1515–1518.

International Seismological Centre (2009), Earthquake hypocentral bulletin, Tech. report, Thatcham, U. K. (Available at http://www.isc.ac.uk.)

Kanamori, H. (1972), Mechanism of tsunami earthquakes, *Phys. Earth Planet. Inter.*, *6*, 346–359.

Kanamori, H., and L. Rivera (2006), Energy partitioning during an earthquake, in *Earthquakes: Radiated Energy and the Physics of Faulting*, *Geophys. Monogr. Ser.*, vol. 170, edited by R. Abercrombie, A. McGarr, H. Kanamori, and G. Di Toro, pp. 3–13, AGU, Washington, D. C.

Lomax, A., A. Michelini, and A. A. Piatanesi (2007), An energy-duration procedure for rapid determination of earthquake magnitude and tsunamigenic potential, *Geophys. J. Int.*, *170*, 1195–1209, doi:10.1111/j.1365-246X.2007.03469.x.

Newman, A. V., and E. A. Okal (1998), Teleseismic estimates of radiated seismic energy: The E/M_0 discriminant for tsunami earthquakes, *J. Geophys. Res.*, *103*, 26,885–26,898.

Newman, A. V., G. Hayes, Y. Wei, and J. A. Convers (2011a), The 25 October 2010 Mentawai tsunami earthquake, from real-time discriminants, finite-fault rupture, and tsunami excitation, *Geophys. Res. Lett.*, *38*, L05302, doi:10.1029/2010GL046498.

Newman, A. V., L. Feng, Z. M. Lifton, H. Fritz, N. Kalligeris, and Y. Wei (2011b), The energetic 2010 M_W 7.1 Solomon Islands tsunami earthquake, *Geophys. J. Int.*, *186*, 775–781, doi:10.1111/j.1365-246X.2011.05057.x.

Ni, S., H. Kanamori, and D. Helmberger (2005), Energy radiation from the Sumatra earthquake, *Nature*, *434*, 582, doi:10.1038/434582a.

Okal, E. A., and A. V. Newman (2001), Tsunami earthquakes: The quest for a regional signal, *Phys. Earth Planet. Inter.*, *124*, 45–70.

Perez-Campos, X., and G. Beroza (2001), An apparent mechanism dependence of radiated seismic energy, *J. Geophys. Res.*, *106*, 11,127–11,136.

Polet, J., and H. Kanamori (2000), Shallow subduction zone earthquakes and their tsunamigenic potential, *Geophys. J. Int.*, *142*, 684–702.

Press, W. H., S. A. Teukolsky, W. T. Vetterling, and B. P. Flannery (1992), *Numerical Recipes in FORTRAN*, 935 pp., Cambridge Univ. Press, New York.

Protti, M., F. Gundel, and K. McNally (1994), The geometry of the Wadati-Benioff zone under southern Central America and its tectonic significance: Results from a high-resolution local seismographic network, *Phys. Earth Planet. Inter.*, *84*, 271–287.

Sahal, A., B. Pelletier, J. Chatelier, and F. Lavigne (2010), A catalog of tsunamis in New Caledonia from 28 march 1875 to 30 September 2009, *C. R. Geosci.*, *342*, 434–447, doi:10.1016/j.crte.2010.01.013.

Schorlemmer, D., S. Wiemer, and M. Wyss (2005), Variation in earthquake-size distribution across different stress regimes, *Nature*, *437*, 539–542, doi:10.1038/nature04094.

Stein, S., and M. Wysession (2003), *An Introduction to Seismology, Earthquakes, and Earth Structure*, Blackwell, Malden, Mass.

Tsuboi, S., K. Abe, K. Takano, and Y. Yamanaka (1995), Rapid determination of M_w from broadband *P* waveforms, *Bull. Seismol. Soc. Am.*, *85*, 606–613.

Tsuboi, S., P. Whitmore, and T. Sokolowski (1999), Application of M_wp to deep and teleseismic earthquakes, *Bull. Seismol. Soc. Am.*, *89*, 1345–1351.

Vassilou, M. S., and H. Kanamori (1982), The energy release in earthquakes, *Bull. Sesimol. Soc. Am.*, *72*, 371–387.

Venkataraman, A., and H. Kanamori (2004), Effect of directivity on estimates of radiated seismic energy, *J. Geophys. Res.*, *109*, B04301, doi:10.1029/2003JB002548.

Vidale, J., and H. Houston (1993), The depth dependence of earthquake duration and implications for rupture mechanisms, *Nature*, *365*, 45–47, doi:10.1038/365045a0.

Weinstein, S. A., and E. A. Okal (2005), The mantle magnitude M_m and the slowness parameter θ: Five years of real-time use in the context of tsunami warning, *Bull. Seismol. Soc. Am.*, *95*, 779–799, doi:10.1785/0120040112.

Wyss, M., and J. Brune (1968), Seismic moment stress and source dimensions for earthquakes in California-Nevada region, *J. Geophys. Res.*, *73*, 4681–4694.

J. A. Convers and A. V. Newman, Department of Earth and Atmospheric Sciences, Georgia Institute of Technology, 311 Ferst Dr., Atlanta, GA 30332-0340, USA. (jaime.convers@eas.gatech.edu; anewman@gatech.edu)